Redox Biology 21 (2019) 101085

Contents lists available at ScienceDirect

Redox Biology

journal homepage: www.elsevier.com/locate/redox

Specific delivery of delta-5-desaturase siRNA *via* RNA nanoparticles supplemented with dihomo-γ-linolenic acid for colon cancer suppression

Yi Xu[a], Lizhi Pang[a], Hongzhi Wang[b,c,d], Congcong Xu[b,c,d], Harshit Shah[a], Peixuan Guo[b,c,d], Dan Shu[b,c,d], Steven Y. Qian[a,*]

[a] Department of Pharmaceutical Sciences, North Dakota State University, Fargo, ND, USA
[b] Center for RNA Nanobiotechnology and Nanomedicine, The Ohio State University, Columbus, OH, USA
[c] College of Pharmacy, Division of Pharmaceutics and Pharmaceutical Chemistry, The Ohio State University, Columbus, OH, USA
[d] College of Medicine, Dorothy M. Davis Heart and Lung Research Institute and James Comprehensive Cancer Center, The Ohio State University, Columbus, OH, USA

ARTICLE INFO

Keywords:
RNA 3WJ nanoparticle
Knockdown of delta-5-desaturase
COX-2-catalyzed DGLA peroxidation
Tumor suppression
HCA-7 colony 29 cells

ABSTRACT

We have previously demonstrated that DGLA treatment along with Delta-5-Desaturase (D5D) siRNA in various types of cancer cells enhances the formation of 8-HOA from COX-2-catalyzed DGLA peroxidation, which in turn inhibits cancer cell growth and migration. However, delivery of naked siRNA remains a formidable challenge due to its "off-target" effect. In this study, we employed RNA nanotechnology for specific delivery of D5D-siRNA to xenograft colon tumors using 3WJ RNA nanoparticles. When a targeting module, *i.e.*, the EpCAM aptamer, was incorporated, the 3WJ pRNA nanoparticles were able specifically deliver D5D siRNA to human colon cancer HCA-7 cells both *in vitro* and *in vivo*, resulting in significant downregulation of D5D expression. Co-treatment with DGLA in combination with 3WJ-EpCAM-siRNA induced a higher DGLA/AA ratio and enhanced formation of 8-HOA at a threshold level, and in HCA-7 tumor-bearing mice, induced significant tumor suppression. We further confirmed that 8-HOA formation, promoted by COX-2-catalyzed DGLA peroxidation, inhibited HDAC and consequently induced apoptosis in tumor cells. Therefore, the 3WJ RNA nanoparticle system holds great promise as a suitable therapeutic delivery platform for colon cancer therapy.

1. Introduction

With more than 9 million new cases estimated for 2018, colon cancer remains one of the most common malignancies in US [1]. However, efficacious treatment of colon cancer with minimum side-effects is still challenging. To achieve specific cancer targeting and drug delivery, a variety of nanodelivery systems have been developed including polymers, lipid nanoparticles, inorganic nanoparticles, micelles, *etc*. [2–11]. Of note, RNA nanotechnology-based delivery systems have shown great potential for targeted therapeutic delivery. The concept of RNA nanotechnology was first evidenced in 1998 by construction of RNA architectures *via* bottom-up self-assembly using the packaging RNA (pRNA) derived from a bacteriophage phi29 DNA packaging motor [12]. Since then, a plethora of RNA nanoparticles have been developed as nanocarriers for drug delivery by virtue of their remarkable chemical/thermodynamic stability and ability to conjugate with various targeting and therapeutic modules [13–21]. More recently, the three-way-junction (3WJ) RNA motif derived from pRNA has been exploited as an ultra-stable core for specifically delivering therapeutic agents (*e.g.*, siRNA, miRNA and small molecules) to different tumors with favorable *in vivo* biodistribution profiles and therapeutic outcomes [22–24].

Recent studies from the Qian group revealed that the COX-2-catalyzed peroxidation of dihomo-γ-linolenic acid (DGLA, an upstream ω-6 fatty acid) can produce a distinct anti-cancer byproduct, 8-hydroxyloctanoic acid (8-HOA), which may act as a histone deacetylase inhibitor (HDACi) in an autocrine manner to suppress cancer cell/tumor growth and migration [25–34]. However, DGLA can be effectively converted to its downstream ω-6 fatty acid arachidonic acid by delta-5-desaturase (D5D), which greatly restricts DGLA's bioavailability. Thus, a D5D knockdown strategy (*via* siRNA transfection) was proposed and demonstrated to successfully limit the conversion from DGLA to arachidonic acid and promote 8-HOA formation, thereby inhibiting cancer cell growth and migration [29–34]. The promoted 8-HOA was found to

Abbreviations: AA, arachidonic acid; COX, Cyclooxygenase; DGLA, dihomo-γ-linolenic acid; D5D, delta-5-desaturase; HCA-7/C29, HCA-7 colony 29 cells; HDAC, histone deacetylase; 3WJ nanoparticle, three way junction nanoparticle; 8-HOA, 8-hydroxyoctanoic acid

* Corresponding author.
E-mail address: steven.qian@ndsu.edu (S.Y. Qian).

https://doi.org/10.1016/j.redox.2018.101085
Received 31 October 2018; Received in revised form 11 December 2018; Accepted 17 December 2018
Available online 18 December 2018

induce p53-dependent apoptosis and cause DNA damage as a result of inhibiting histone deacetylase (HDAC) in various types of cancer [29–34].

However, the successful translation of D5D siRNA for cancer treatment is hindered by its "off-target" effects, *in vivo* instability, and susceptibility to degradation [35–37]. Hence, development of a suitable nanocarrier to improve the therapeutic efficacy of D5D-siRNA is an urgent need. In the present study, we report the first endeavor to design and employ 3WJ RNA nanoparticles for specific D5D-siRNA delivery to colon cancer. Our flow cytometry analysis and confocal microscopy imaging results showed that as a targeting ligand, the EpCAM aptamer facilitated the specific binding and entry of 3WJ-D5D siRNA nanoparticles into human colon cancer HCA-7 cells *in vitro*. The nanoparticle *in vivo* biodistribution profile further confirmed the specific targeting of 3WJ-EpCAM nanoparticles to colon cancer after systemic injection. *In vivo* therapeutic effects were evaluated by monitoring the tumor growth after co-treatment with DGLA and 3WJ nanoparticles harboring EpCAM aptamer and D5D-siRNA. Significant suppression of tumor growth in HCA-7 tumor-bearing mice was observed and further confirmed at the tissue and molecular level by immunofluorescence analysis and western blot. Therefore, the 3WJ-EpCAM nanoparticle delivery system provides a potential new treatment strategy for colon cancer therapy.

2. Materials and methods

2.1. Reagents and materials

Analytical standard grades of AA, DGLA, AA-d_8 and DGLA-d_6 as well as DGLA ethyl ester (used for animal supplements) were purchased from Cayman Chemical (MI, USA). Pentafluorobenzyl bromide, diisopropylethylamine, HPLC-MS grade water, acetonitrile, acetic acid and methanol were obtained from VWR (PA, USA). A SampliQ Silica C18 ODS reverse phase SPE cartridge was obtained from Agilent Technology (CA, USA). T-Per tissue protein extraction reagent was bought from Thermo Fisher Scientific (MA, USA). Fetal bovine serum (FBS) and Dulbecco's Modified Eagle's Medium were obtained from VWR (PA, USA). For immunofluorescence studies, primary antibodies for D5D, cleaved PARP, Ki-67, and Alexa fluor-conjugated secondary antibodies were acquired from Abcam (MA, USA). For western blot experiments, γH2AX primary antibody was purchased from Bethyl Laboratories (TX, USA). Primary antibodies for p53, Bcl-2, acetyl histone H3, procaspase 9, β-actin, and horseradish peroxidase-conjugated secondary antibodies were bought from Cell Signaling (MA, USA). D5D-targeted siRNA strands were synthesized and obtained from Integrated DNA Technologies (IA, USA); the sequences are as follows: sense strand 5′ uuG ccA uGu GuA uGu GGG uuA cAu cAu ccA cuc Acu AAA tt 3′ (lowercase indicate 2′-fluoro RNA); antisense strand: 5′ UUU AGU GAG UGG AUG AUG UCG 3′. Alexa 647 NHS ester was purchased from Thermo Fisher (USA). Phosphoramidites and synthesizer reagents for solid-phase RNA synthesis were obtained from Glen Research (USA). RT-PCR master mix and mRNA reverse transcription systems were purchased from Promega (WI, USA). A Qiagen RNA mini Prep kit was obtained from Qiagen (USA).

2.2. Cancer cell line

The human colon cancer cell line HCA-7 colony 29 (from the European Collection of Cell Cultures) was grown in Dulbecco's Modified Eagle's Medium supplemented with 10% FBS. Cells were cultured in an incubator with a 95% humidified atmosphere and 5% CO_2 at 37 °C.

2.3. Synthesis of 3WJ nanoparticles

3WJ RNA nanoparticles were constructed using a bottom-up approach. 3WJ-EpCAM-D5D siRNA nanoparticles consisted of four fragments harboring EpCAM19 aptamers as targeting ligands and D5D target siRNA as the therapeutic agent. The control included RNA nanoparticles without the therapeutic module. In a biodistribution study, Alexa 647 as an imaging probe was conjugated to 3WJ nanoparticles. All the strand sequences are described below. Lowercase letters indicate 2′-F modified nucleotides:

a_{3WJ}: 5′- uuG ccA uGu GuA uGu GGG −3′
a_{3WJ}: D5D sense strand: 5′- uuG ccA uGu GuA uGu GGG uuA cAu cAu ccA cuc Acu AAA tt −3′
b_{3WJ}-EpCAM: 5′- ccc AcA uAc uuu Guu GAu ccu uuG Cga cuG Guu Acc cGG ucG-3′
c_{3WJ}: 5′- GGA ucA Auc AuG GcA A −3′
c_{3WJ}-Alexa 647: 5′- GGA ucA Auc AuG GcA A(C6-NH) (Alexa 647) −3′
D5D antisense strand: 5′-UUU AGU GAG UGG AUG AUG UCG-3′

D5D-targeted siRNA strands were synthesized and obtained from Integrated DNA Technologies (IA, USA). Short RNA oligomer (3WJa, 3WJc) synthesis was conducted on a 200 nmole scale universal column on an automated oligo synthesizer ASM-800E from Biosset (Russia). Coupling efficiency was monitored after removal of the dimethoxytrityl (DMT) protecting groups. 3WJc strands were 5′ modified with a primary amine (cat. No: 10-1947-90, Glen Research). Conjugation of Alexa 647 on 3WJc *via* an NHS ester reaction was carried out by mixing a 1:10 M ratio of primary amine modified RNA: Alexa 647 NHS ester in 0.1 M sodium bicarbonate buffer, with alkaline pH (~8.5). The conjugation reactions were incubated at room temperature for 4 h while protected from light. Following incubation, the reaction solutions were ethanol precipitated and washed twice with cold 75% ethanol to remove the unreacted fluorophore, followed by reverse phase HPLC purification.

Assembly of 3WJs was performed by mixing corresponding strands at equimolar molar concentration in TES buffer (10 mM TRIS pH = 7.5, 50 mM NaCl, 1 mM EDTA) and annealing at 85 °C for 5 min followed by slow cooling to 4 °C over about 50 min. 3WJ nanoparticle formation was confirmed on a 12% native PAGE in TBE running buffer (89 mM Tris, 200 mM boric acid, and 5 mM $MgCl_2$). Gels were stained with ethidium bromide (EtBr) followed by imaging by Typhoon FLA 7000 (GE Healthcare).

2.4. Dynamic light scattering measurements

The apparent hydrodynamic sizes of the assembled RNA nanoparticles (40 μM in 1 × Tris buffer) were measured by a Zetasizer nano-ZS (Malvern Instrument, LTD) at 25 °C. The laser wavelength used for the experiments was 633 nm. The data were obtained from at least three independent measurements.

2.5. Atomic force microscopy

Extended RNA 3WJ nanoparticles were imaged by a Veeco MultiMode AFM NanoScope IV system using APS-treated mica following previously reported procedures [38]. Mica was freshly cleaved and immersed in an aqueous solution of 1-(3-aminopropyl)-silatrane (APS) for 30 min. The APS-treated mica pieces were rinsed in deionized water and dried under a flow of high purity argon, followed by vacuum drying for at least 12 h. A droplet of diluted RNA sample in 1 x Tris buffer was deposited onto APS-treated mica for 2 min. Then the mica surface was rinsed briefly using deionized water and dried with a gentle flow of argon. Images was taken with a MultiMode AFM Nanoscope IV system (Bruker Instruments, USA) in Tapping Mode and processed using the NanoScope Analysis software (Veeco Instruments Inc).

2.6. Flow cytometry analysis for cell binding of 3WJ nanoparticles

About 3×10^5 HCA-7 cells were trypsinized and washed with PBS.

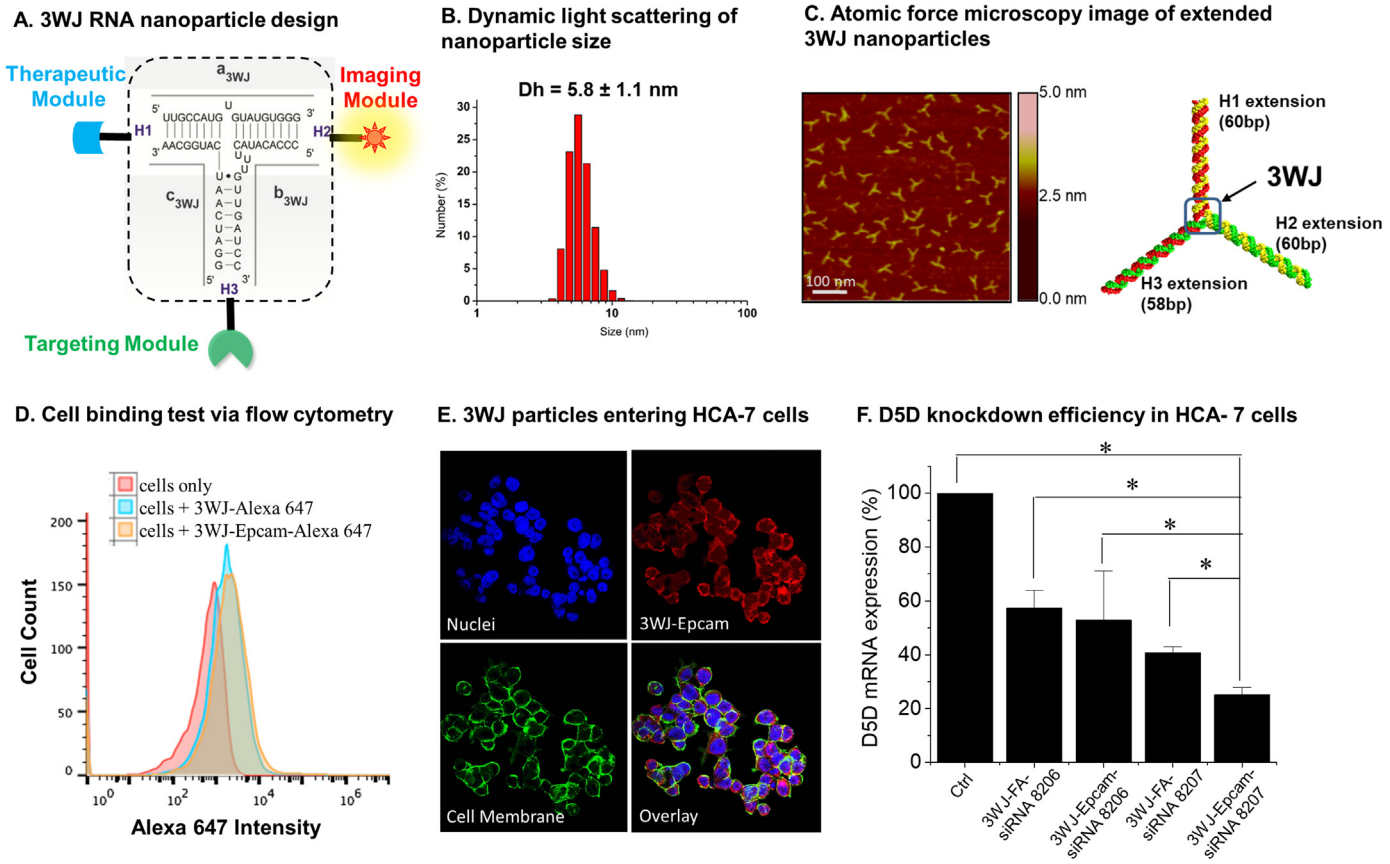

Fig. 1. Construction of tumor-targeting 3WJ nanoparticle. (A) Illustration for the design of a functional 3WJ RNA nanoparticle. (B) Dynamic light scattering characterization showing the hydrodynamic size of RNA nanoparticles. (C) Atomic force microscopy image of extended 3WJ-nanoparticles. (D) Cell-binding test *via* flow cytometry in HCA-7/C29 cells after being incubated with 100 nM 3WJ-Alexa 647 or 3WJ-EpCAM-Alexa 647 (in 100 μL PBS). Cells incubated with PBS only (without nanoparticles) served as controls. (E) Confocal microscopy analysis of 3WJ-EpCAM-Alexa 647 particles entering HCA-7/C29 cells. Cell skeletons were stained with Alexa 488 and cell nuclei with DAPI. (F) qRT-PCR analysis for D5D gene knockdown efficiency in HCA-7/C29 cells after treatment with 10 nM of 3WJ nanoparticles with different compositions. Data represent mean ± SD with three separate experiments. *: significant difference with $p < 0.05$.

The cells were then centrifuged and suspended in either 100 nM 3WJ-Alexa 647 or 3WJ-EpCAM-Alexa 647 (in 100 μL PBS). Cells incubated with PBS only (without nanoparticles) served as a control. After a 2 h incubation at 37 °C, the cells were washed and re-suspended in 100 μL PBS, followed by flow cytometry analysis for Alexa 647 intensity.

2.7. Confocal microscopy imaging analysis

Acid-washed cover glasses were placed in each well on a 24-well plate. Then ~50,000 HCA-7 cells were seeded in each well and incubated overnight. After removing the cell culture medium, the cells were incubated with 100 nM 3WJ-EpCAM-Alexa 647 nanoparticles in 200 μL of serum-free medium for 2 h. The cells were then washed with PBS and fixed in formaldehyde for 30 min. Alexa 488 and DAPI were added in each well for cell skeleton and nuclei staining, respectively. The cover glasses were placed on slides and air-dried overnight for confocal microscopy analysis using a Zeiss Axio Observer Z1 LSM 700.

2.8. Quantitative RT-PCR analysis

D5D gene knockdown efficiency after 3WJ-siRNA nanoparticle treatment was assessed by qRT-PCR analysis. Briefly, HCA-7 cells were seeded at 1×10^5 per well in a 24 well plate overnight, then incubated with 10 nM 3WJ-siRNA nanoparticles for 48 h. The cells were trypsinized, centrifuged, and washed with PBS, followed by RNA extraction using a Qiagen RNA mini Prep kit according to the manufacturer's instructions. The RNA extracts were reverse transcribed to cDNA and subjected to qRT-PCR analysis for D5D mRNA levels. The sequence for D5D and 18s rRNA (internal standard) primers are as follows: D5D reverse primer, 5′-AGTCTTCCTCCTCTTCTTCCA-3′, D5D forward primer, 5′-CCGACATCATCCACTCACTAAA-3′. 18s reverse primer, 5′-GCCTCGAAAGAGTCCTGTATTG-3′, and 18s forward primer, 5′-CTG AGAAACGGCTACCACATC-3′.

2.9. Mouse xenograft tumor model and treatment

Six-week old female and male nude mice (J:Nu, stock number 007850) were purchased from The Jackson Laboratory (Bar Harbor, ME). The mice, five per cage, were housed in a pathogen-free Innovive IVC system with water and food *ad libitum*. All the animal experiments were approved by the Institutional Animal Care and Use Committees at North Dakota State University. After allowing the mice to acclimatize for one week, tumor xenografts were established by subcutaneously injecting 2×10^6 HCA-7/C29 cells (suspended in 100 μL PBS) into the hind flank of each mouse. The mice were then fed a standard diet for two more weeks to allow the tumors to grow, and divided into four groups (6 mice per group) for four-week treatments: (1) vehicle control; (2) DGLA ethyl ester at a dose of 8 mg/mouse, oral gavage, twice a week; (3) 3WJ-EpCAM-siRNA, 20 μM in 50 μL PBS, *i.v.* injection, twice a week; and (4) both DGLA ethyl ester and 3WJ-EpCAM-siRNA.

2.10. Biodistribution analysis

The mice bearing HCA-7/C29 tumors were injected with 3WJ-EpCAM-Alexa 647 or vehicle control (PBS) for 8-h, then the mice were euthanized, and organs and tumor tissues were collected for

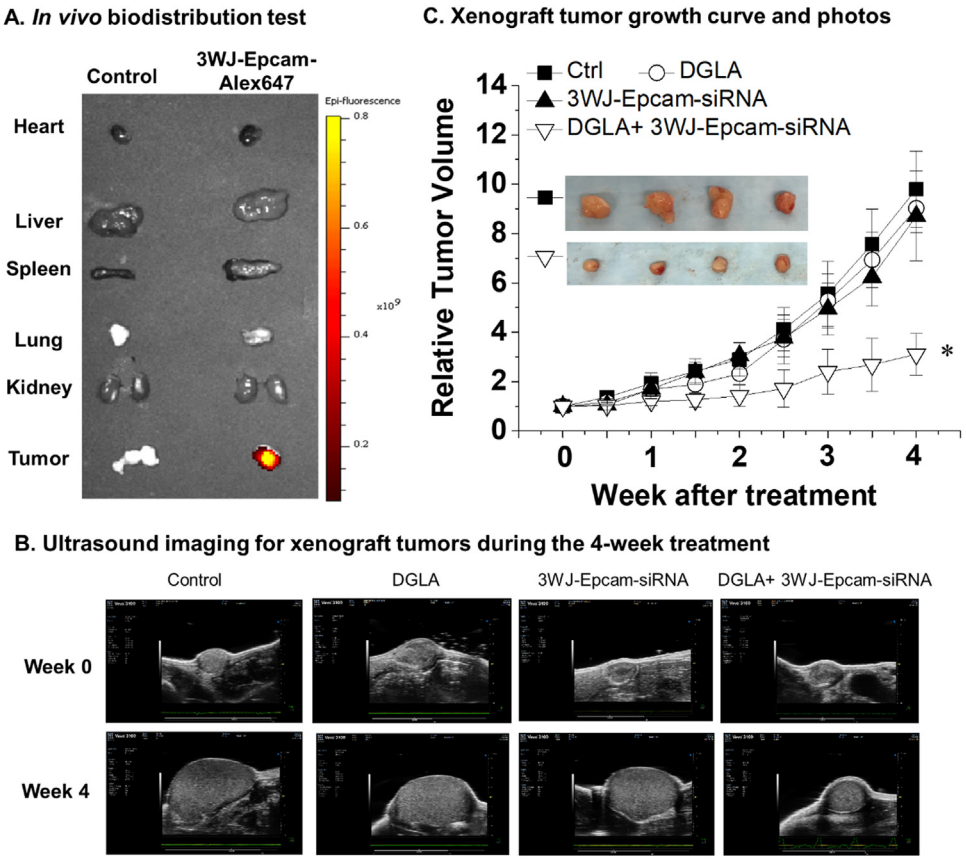

Fig. 2. 3WJ nanoparticles and DGLA supplementation suppress xenograft tumor growth. (A) *In vivo* biodistribution analysis of 3WJ-EpCAM-Alexa 647 particles in organs and tumor tissues from mice bearing HCA-7 tumors at 8-h post-injection. (B) Ultrasound images of tumor growth in mice before and after 4-week treatments. Note, week 0 indicates the starting point of treatment, which is two weeks after cancer cell implantation. (C) Relative tumor volume measured twice a week using a digital caliper during the treatment. Data represent mean ± SD with six tumor samples. *: significant difference with $p < 0.05$. Insert: photos of tumor tissues at the end of treatment.

biodistribution analysis using the IVIS Lumina Series III Pre-clinical In Vivo Imaging System (Perkin Elmer).

2.11. Tumor size measurement

Tumor growth was monitored twice a week using a digital caliper during the treatment. Tumor volume was calculated as: $V = L \times W^2/2$. In addition, a Vevo 3100 ultrasound imaging system (FUJIFILM VisualSonics) was used to record tumor growth weekly. At the endpoint, the mice were euthanized with an overdose of pentobarbital (200 mg/kg, *i.p.*) and the tumor tissues were collected for further analysis.

2.12. Quantification of DGLA and AA in tumor tissues

The free DGLA and AA in tumor tissues were quantified *via* LC/MS analysis as described elsewhere [33,34]. Briefly, tumor tissues (~50–100 mg) were weighed, frozen in liquid nitrogen, and crushed to fine powders. The powders were then mixed with water and methanol as well as internal standards (AA-d_8 and DGLA-d_6). The mixtures were vortexed for 1 min and set on ice for 30 min, followed by the extraction procedures as described our previous report [25–34].

The LC/MS system, consisting of an Agilent 1200 series HPLC system and an Agilent 6300 LC/MSD SL ion trap MS, was used to quantify the free fatty acids in tumor samples. For quantification, an internal standard curve was constructed from a series of mixtures consisting of DGLA and AA standard solutions at various concentrations, and the internal standards at a constant concentration. The concentrations of fatty acids in the samples were calculated using the internal standard curve by comparing the ratios of the peak areas of the analytes to the peak areas of their corresponding internal standards.

2.13. GC/MS analysis of 8-HOA

8-HOA produced from tumor cells was quantified *via* GC/MS analysis as its derivative of pentafluorobenzyl bromide (PFB-Br) as described elsewhere [29–34,39]. Briefly, tumor tissues (~50–100 mg) frozen in liquid nitrogen were crushed to powders and suspended in 1.0 mL water. The suspension was mixed with 500 μL of methanol containing an internal standard (hexanoic acid), 50 μL of 1.0 N HCl, and 3.0 mL of dichloromethane, followed by the same procedures as described in our previous report [29–34].

The sample solutions (2.0 μL) were injected into an Agilent 7890 A gas chromatograph. The GC oven temperature was programmed from 60 to 300 °C at 25 °C/min. The injector and transfer line were kept at 280 °C. Quantitative analysis was performed using a mass selective detector with a source temperature of 230 °C. For quantification, an internal standard curve was constructed from a series of mixtures consisting of 8-HOA at various concentrations and the internal standard hexanoic acid at a constant concentration. The concentrations of 8-HOA in the samples were calculated using the internal standard curve by comparing the ratio of the peak area of the 8-HOA to the peak area of the internal standard.

2.14. Immunofluorescence analysis

The expression of D5D, cleaved PARP and Ki-67 in tumor tissues was analyzed by immunofluorescence at the Advanced Imaging & Microscopy Laboratory, NDSU. Briefly, freshly collected tumor tissues were fixed with 10% formaldehyde and embedded in paraffin blocks. Tissue sections were deparaffinized with xylene, rinsed, and rehydrated through a graded series of alcohol. For antigen retrieval, the slides were placed in a rack in the retriever (Aptum Biologics Ltd, UK) filled with sodium citrate buffer, and the retriever was run for 30 min at preset pressure and temperature. Then the tumor sections were incubated with

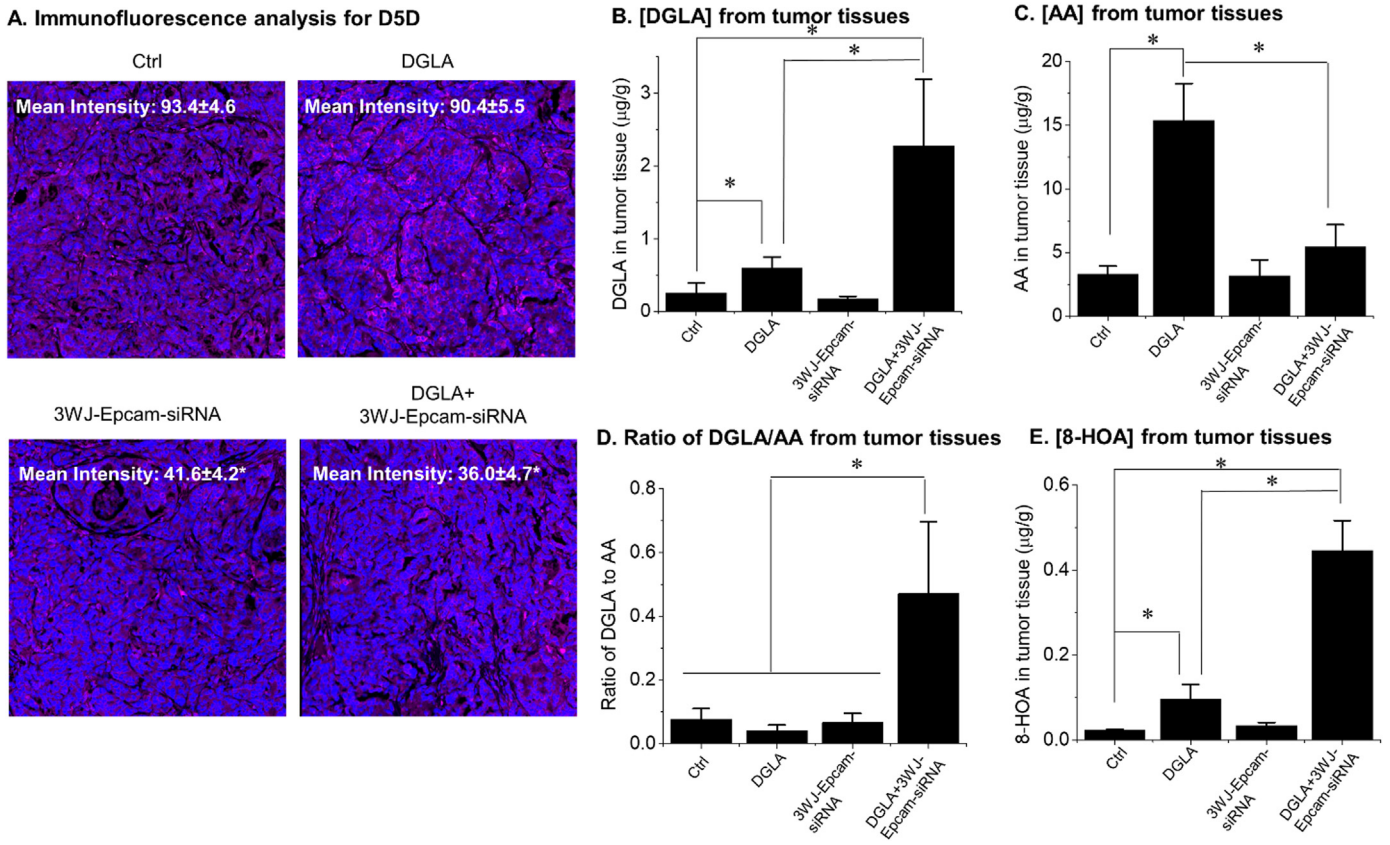

Fig. 3. 3WJ nanoparticles and DGLA supplementation promote 8-HOA formation in xenograft tumors. (A) Immunofluorescence analysis of D5D expression levels in tumor tissues. (B) LC/MS quantification of DGLA levels from tumor tissues. (C) LC/MS quantification of AA levels from tumor tissues. (D) DGLA/AA ratio from tumor tissues. (E) GC/MS quantification of 8-HOA from tumor tissues. All the quantification data represent mean ± SD with six tumor samples. *: significant difference with $p < 0.05$.

primary antibodies and subsequently with fluorochrome-conjugated secondary antibodies. Cell nuclei were counter-stained with DAPI. The images were acquired with a Zeiss Axio Imager M2 microscope.

Expression levels of D5D in tumors were quantified *via* mean fluorescence intensities using Image Pro software (Media Cybernetics, Inc. Rockville, MD). The expression levels of cleaved PARP were presented as the percentage of cleaved PARP-positive cells *vs*. the total number of tumor cells. Similarly, the percentage of Ki-67 positive events relative to the total number of events was used for the quantification of the expression level of Ki-67.

2.15. Western blot analysis

The expression of p53, Bcl-2, procaspase 9, γH2AX and acetyl histone H3 in tumor tissues was assessed by western blot. Tumor tissues (~50–100 mg) were frozen in liquid nitrogen and crushed to fine powders, then the protein was extracted using T-Per tissue protein extraction reagent. The same amount of protein from each sample was then loaded into 10% SDS-PAGE gels. The gels were run at a constant current of 30 mA for 1 h, and proteins were then transferred to nitrocellulose membranes at a constant voltage of 80 V for 2 h on ice. The membranes were incubated with primary antibodies overnight at 4 °C and horseradish peroxidase-conjugated secondary antibody for 1 h at room temperature with continuous rocking. Then the membranes were incubated in ECL western blot substrates for 2 min, followed by exposure to X-ray film. Luminescent signals were captured on a Mini-Medical Automatic Film Processor (Imageworks).

2.16. Statistics

Data were presented as mean ± SD from six tumor samples per treatment group. Statistical differences between the mean values for different groups were evaluated by student *t*-test; differences were considered significant with a p-value < 0.05.

3. Results

3.1. Characterization of 3WJ nanoparticles

The 3WJ motif derived from pRNA molecule can be used as a scaffold to simultaneously harbor different modules including a therapeutic agent, tumor targeting ligand and imaging probe (Fig. 1A). Here we designed and synthesized 3WJ particles to specifically deliver D5D-siRNA to colon cancer cells. Upon mixing the corresponding strands in an equal molar ratio in TES buffer, the nanoparticles assemble with high efficiency (Supplemental Fig. 1). Dynamic light scattering measurements revealed that the size of the RNA nanoparticles was 5.8 ± 1.1 nm (Fig. 1B). Due to the resolution limit of the atomic force microscopy (AFM) probe, the size of the constructed 3WJ nanoparticles was too small to be imaged with detailed structure and shape. To evaluate the branch structure of the constructed RNA nanoparticles, extended 3WJ nanoparticles with 60 bp of dsRNA extension on the a, b, and c arms respectively were used for AFM imaging (Fig. 1C). It is expected that 60 bp of dsRNA extension maintains the global structure of the resulting RNA nanoparticles derived from the 3WJ motif since it is within the persistence length of 229 bp [40].

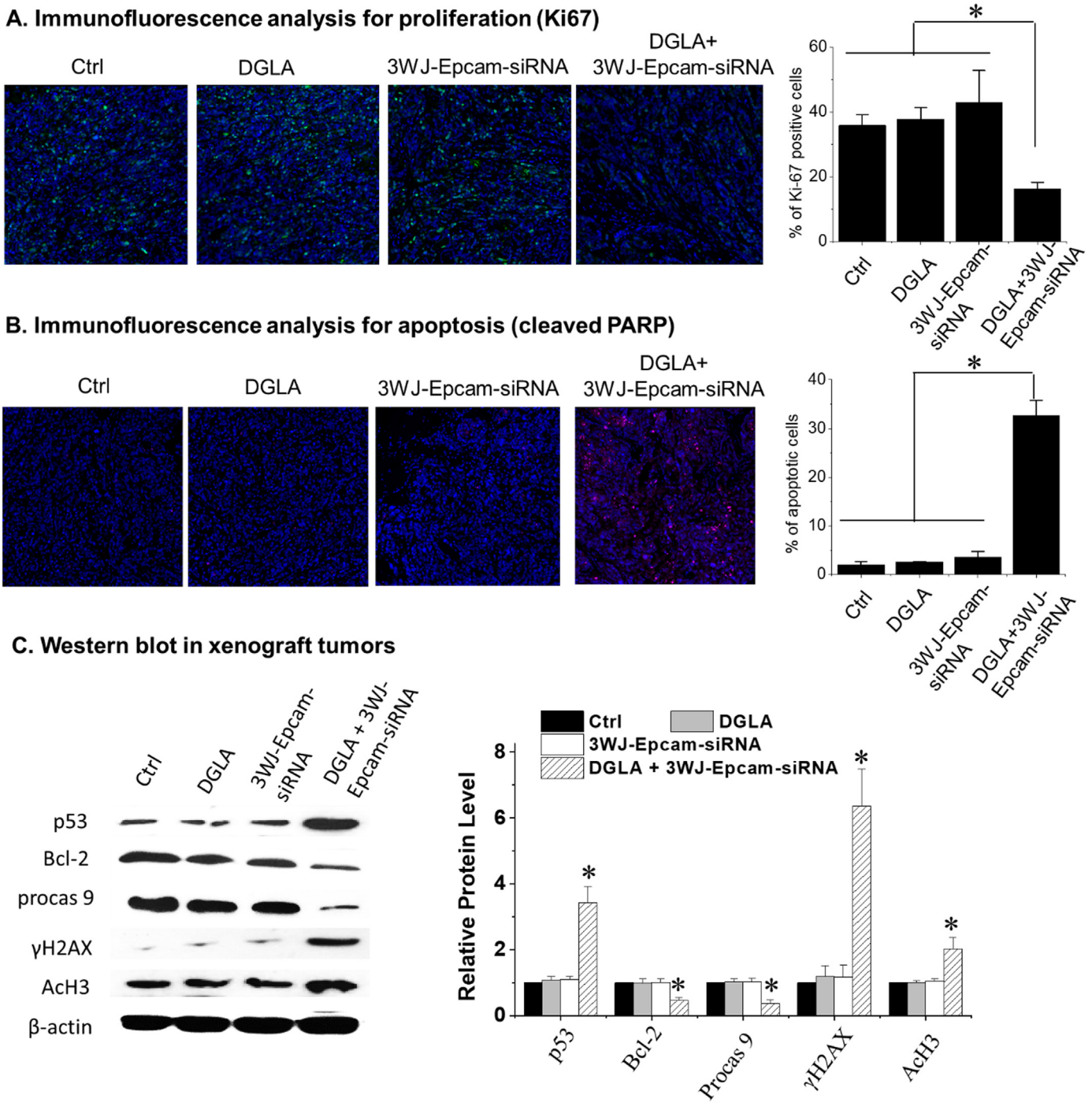

Fig. 4. Promoted 8-HOA formation inhibits HDAC and induces apoptosis in tumor cells. (A) Immunofluorescence analysis for Ki-67 expression in tumor tissues. Ki-67 was stained in green, cell nuclei were counter-stained with DAPI. (B) Immunofluorescence analysis for cleaved PARP expression in tumor tissues. Expression of cleaved PARP was stained in red, and cell nuclei were counter-stained with DAPI. (C) Western blot and relative protein expression levels of p53, bcl-2, procaspase 9, acetyl histone H3 and γH2AX in tumor tissues. β-actin served as a loading control. The ratio of each protein to β-actin in the controls was normalized. Note, the p53 is heterogeneous in HCA-7 cells with both wild type and mutant isoforms present. Here only the bands from wild type p53 was shown while its truncated isoform (~40 KD) was not shown. All the quantification data represent mean ± SD with six tumor samples. *: significant difference with $p < 0.05$.

3.2. 3WJ-EpCAM-siRNA nanoparticles inhibit D5D expression in cancer cells in vitro

Flow cytometry data demonstrated that, by conjugating with EpCAM aptamer (a tumor targeting module for colon cancer cells), the 3WJ-EpCAM nanoparticles bound to EpCAM-positive HCA-7/C29 cells more efficiently than 3WJ particles without any targeting module (Fig. 1D). Confocal microscopy analysis also confirmed that the 3WJ-EpCAM nanoparticles can enter HCA-7/C29 cells efficiently (Fig. 1E). PCR analysis was performed to evaluate the gene knockdown efficiency in HCA-7/C29 cells exposed to 3WJ nanoparticles with different tumor targeting modules (EpCAM vs folic acid) and D5D siRNA strands (siRNA 8206 vs 8207). Results revealed that the composition of 3WJ-EpCAM-si8207 showed most efficient D5D knockdown activity, therefore we used this composition for the following experiments (Fig. 1F).

3.3. 3WJ-EpCAM-siRNA accumulate in xenograft tumors and suppress tumor growth

The mice bearing HCA-7/C29 tumors were injected with 3WJ-EpCAM-Alexa 647 or vehicle control (PBS), then after 8 h, the mice were euthanized, and organs and tumor tissues were collected for biodistribution analysis. Results showed that the nanoparticles specifically accumulated in tumor tissues 8-hr after injection while being cleared in other organs (Fig. 2A).

We then tested the potential anti-tumor effect of a combination treatment of a DGLA supplement along with 3WJ-EpCAM-D5D siRNA in mice bearing HCA-7/C29 tumors. Data showed that the combination treatment significantly inhibited xenograft tumor growth (~65% inhibition at week 4) compared to the control group as well as to DGLA treatment only and nanoparticle treatment only (Fig. 2B-C). We also tested the effect from the combination of DGLA with naked siRNA. As we expected, without nanoparticle formulation, there was no significant inhibitory effect observed (data not shown), probably due to the rapid degradation of naked siRNA.

3.4. 3WJ-EpCAM-siRNA and DGLA treatment promotes 8-HOA formation in vivo

Immunofluorescence data showed that 3WJ-EpCAM-siRNA treatment significantly knocked down D5D expression in tumor tissues compared to those without nanoparticle treatment (Fig. 3A). Consistently, concurrent application of 3WJ-EpCAM-siRNA resulted in significantly increased DGLA levels and decreased AA in tumors compared to DGLA supplementation alone (Fig. 3B-C). As a result, the ratio of DGLA to AA from the combination treatment group was significantly higher than any other group (Fig. 3D).

More importantly, in the mice without DGLA supplementation, only basal levels of 8-HOA were detected in tumors (< 0.03 μg/g, Fig. 3E). In comparison, DGLA treatment only led to a moderate increase of 8-HOA (< 0.1 μg/g), while the combination treatment significantly promoted 8-HOA formation (> 0.4 μg/g,) to reach a possible threshold level for exerting its anti-cancer effects.

3.5. Effect of 3WJ-EpCAM-siRNA and DGLA treatment in tumor proliferation and apoptosis

Immunofluorescence studies were conducted to test whether our strategy could inhibit tumor proliferation and induce apoptosis. Results showed that DGLA supplementation or nanoparticles alone did not have any influence on tumor proliferation, evident by the unchanged expression of Ki-67 (a proliferation marker, Fig. 4A). On the other hand, the combination of DGLA supplementation with 3WJ-EpCAM-siRNA resulted in a significantly decreased expression of Ki-67 in tumor tissues compared to the vehicle control.

Tumor apoptosis was assessed by immunofluorescence analysis of the expression of cleaved PARP (tumor apoptotic marker). Results showed that DGLA supplementation or nanoparticle alone did not induce tumor apoptosis, while DGLA supplementation along with 3WJ-EpCAM-siRNA resulted in significantly increased apoptotic cells in tumor tissues (Fig. 4B).

We also conducted western blotting to investigate the molecular mechanisms by which our strategy could inhibit tumor growth. Data showed that the combination treatment resulted in significantly increased expression of p53 and decreased expression of Bcl-2 and procaspase 9, representing activation of the p53-dependent cell/tumor apoptotic pathway (Fig. 4C). We also observed accumulation of acetyl histone H3 and γH2AX in tumors with the combination treatment, which is consistent with our previous publication concluding that promoted 8-HOA could inhibit HDAC and induce DNA damage [29–34]. In comparison, DGLA supplementation alone or nanoparticles alone failed to activate apoptosis, with no changed HDAC activity, as 8-HOA never reached the threshold level (Fig. 3E).

4. Conclusion and discussion

We had previously demonstrated that DGLA treatment along with D5D knockdown in various types of cancer cells can lead to promoted formation of 8-HOA (an HDAC inhibitor) from COX-2-catalyzed DGLA peroxidation, which in turn inhibited cancer cell growth, migration, and invasion [25–34]. In this study, we have made the first endeavor to design and employ 3WJ RNA nanoparticles for delivering D5D-siRNA specifically to xenograft tumors.

Results showed that when a targeting module, *i.e.*, the EpCAM aptamer, is conjugated to the 3WJ pRNA nanoparticles, they can specifically bind and accumulate in human colon cancer HCA-7 cells and in xenograft tumors. The 3WJ-EpCAM-siRNA significantly inhibited D5D expression *in vitro* and *in vivo*. Results from the animal study demonstrated that co-treatment with DGLA in combination with 3WJ-EpCAM-siRNA can significantly suppress xenograft tumor growth in mice bearing HCA-7 tumors.

Consistent with previous *in vitro* (siRNA) and *in vivo* (shRNA) experiments [29–34], we observed that DGLA treatment along with 3WJ-EpCAM-siRNA inhibited the tumor growth by maintaining a higher DGLA/AA ratio and promoting the formation of 8-HOA at a threshold level (Fig. 3). The body weights of the mice were recorded twice a week during the treatment, and no significant difference was noted among different treatment groups, suggesting no severe toxicity from the treatments (Supplemental Fig. 2). Western blot further confirmed that promoting 8-HOA formation from COX-2-catalyzed DGLA peroxidation resulted in a significant increase of acetyl histone H3 and γH2AX. We demonstrated again that the anti-proliferation effect of DGLA is actually derived from 8-HOA's action to inhibit HDAC and damage DNA in tumor cells [29–34].

3WJ RNA nanoparticles are able to harbor three modules simultaneously for different purposes, including tumor targeting, therapeutic and imaging purposes. In our animal study, for treatment purposes, we synthesized the 3WJ nanoparticles conjugated with only two modules: one targeting module (EpCAM aptamer) and one therapeutic module (D5D-siRNA). Thus, the full potential of 3WJ nanoparticles has not been exploited. In our future studies, we will optimize the composition of nanoparticles, *e.g.*, conjugating 3WJ with different siRNAs and targeting modules to achieve the most effective anti-tumor outcome. In addition, in our ongoing research we are developing small compounds as D5D inhibitors, which may be also conjugated with 3WJ particles for specific tumor delivery.

The successful translation of D5D siRNA for cancer treatment is hindered by its “off-target” effects, *in vivo* instability, and susceptibility to degradation [35–37]. Hence, development of a suitable nanocarrier to improve the therapeutic efficacy of D5D-siRNA is an urgent need. For the first time, we have employed the innovative 3WJ RNA nanoparticles to specifically deliver D5D-siRNA to tumor cells, by virtue of their remarkable chemical/thermodynamic stability. Our data showed that 3WJ-EpCAM-siRNA specifically delivered D5D siRNA to tumor cells and inhibited D5D expression, which then promoted 8-HOA formation from COX-2 catalyzed DGLA peroxidation. The promoted 8-HOA in turn regulated histone deacetylation and induced DNA damage, thereby triggering the activation of the cell apoptosis pathway, and led to tumor growth inhibition. Combining the innovative RNA nanotechnology-based therapy with our paradigm-shifting concept, *i.e.,* knocking down D5D and taking advantage of commonly overexpressed COX-2 in cancer cells, shows a favorable outcome and sheds new light on the development of a promising colon cancer therapy for translation to the clinic.

CRediT authorship contribution statement

Yi Xu: Formal analysis, Investigation, Methodology, Validation, Visualization, Writing - original draft, Writing - review & editing. **Lizhi Pang:** Investigation, Writing - review & editing. **Hongzhi Wang:** Investigation, Methodology, Resources, Writing - original draft, Writing - review & editing. **Congcong Xu:** Investigation, Methodology, Resources. **Harshit Shah:** Investigation. **Peixuan Guo:** Conceptualization, Methodology, Resources, Writing - review & editing. **Dan Shu:** Conceptualization, Funding acquisition, Methodology, Resources, Writing - review & editing. **Steven Y. Qian:** Conceptualization, Funding acquisition, Project administration, Resources, Supervision, Writing - review & editing.

Acknowledgement

We would like to acknowledge use of the Small Animal Core Facility at NDSU for work described in this manuscript. This Core Facility is part of The Center for Diagnostic and Therapeutic Strategies in Pancreatic Cancer and is funded by National Institute of General Medical Sciences of the National Institutes of Health, Award Number 1P20GM109024. The authors would also like to thank the Nanoimaging Core Facility at UNMC for assistance with AFM imaging. The Facility is in part supported by funds received from the Nebraska Research Initiative (NRI).

Declarations

Ethics approval and consent to participate

All the animal experiments were approved by the Institutional Animal Care and Use Committees at North Dakota State University.

Consent for publication

Not applicable.

Availability of data and materials

The datasets used and/or analyzed during the current study are available from the corresponding author on reasonable request.

Competing interests

P.G. is the cofounder of ExonanoRNA LLC. He is also a consultant of Oxford Nanopore Technologies and Nanobio Delivery Pharmaceutical Co. Ltd., as well as the cofounder of Shenzhen P&Z Bio-medical Co. Ltd. and its subsidiary US P&Z Biological Technology LLC. His inventions at the University of Kentucky have been licensed to Matt Holding and Nanobio Delivery Pharmaceutical Co., Ltd. The content is solely the responsibility of the authors and does not necessarily represent the official views of the NIH.

Funding

This work was supported by National Cancer Institute R15CA195499 (Dr. Steven Qian), National Institute of General Medical Sciences P20GM109024 (Center for Diagnostic and Therapeutic Strategies in Pancreatic Cancer, NDSU), and DOD Award W81XWH-15-1-0052 (Dr. Dan Shu).

Authors' contributions

SYQ made substantial contributions to provide funding support, conceptual design, interpretation of data, and writing/editing the manuscript; YX made substantial contributions to data acquisition, analysis and interpretation, and writing/editing the manuscript; LZP, HZW, CCX and HS made substantial contributions to data acquisition, analysis and interpretation; DS and PXG made substantial contributions to conception and design, and interpretation of data. All authors read and approved the final manuscript.

Appendix A. Supporting information

Supplementary data associated with this article can be found in the online version at doi:10.1016/j.redox.2018.101085.

References

[1] R.L. Siegel, K.D. Miller, S.A. Fedewa, D.J. Ahnen, R.G.S. Meester, A. Barzi, A. Jemal, Colorectal cancer statistics, CA Cancer J. Clin. 67 (2017) 177–193.
[2] A.Z. Wang, R. Langer, O.C. Farokhzad, Nanoparticle delivery of cancer drugs, Annu. Rev. Med. 63 (2012) 185–198.
[3] S.D. Steichen, M. Caldorera-Moore, N.A. Peppas, A review of current nanoparticle and targeting moieties for the delivery of cancer therapeutics, Eur. J. Pharm. Sci. 48 (2013) 416–427.
[4] S.M. Moghimi, A.C. Hunter, J.C. Murray, Nanomedicine: current status and future prospects, FASEB J. 19 (2005) 311–330.
[5] D.D. Lasic, Doxorubicin in sterically stabilized liposomes, Nature 380 (1996) 561–562.
[6] M.J. Hawkins, P. Soon-Shiong, N. Desai, Protein nanoparticles as drug carriers in clinical medicine, Adv. Drug Deliv. Rev. 60 (2008) 876–885.
[7] J.R. Baker Jr., Dendrimer-based nanoparticles for cancer therapy, Hematol. Am. Soc. Hematol. Educ. Program (2009) 708–719.
[8] C. Minelli, S.B. Lowe, M.M. Stevens, Engineering nanocomposite materials for cancer therapy, Small 6 (2010) 2336–2357.
[9] R.K. Jain, T. Stylianopoulos, Delivering nanomedicine to solid tumors, Nat. Rev. 7 (2010) 653–664.
[10] M. Wang, M. Thanou, Targeting nanoparticles to cancer, Pharmacol. Res. 62 (2010) 90–99.
[11] A. Gaitanis, S. Staal, Liposomal doxorubicin and nab-paclitaxel: nanoparticle cancer chemotherapy in current clinical use, Methods Mol. Biol. 624 (2010) 385–392.
[12] P. Guo, C. Zhang, C. Chen, K. Garver, M. Trottier, Inter-RNA interaction of phage phi29 pRNA to form a hexameric complex for viral DNA transportation, Mol. Cell 2 (1998) 149–155.
[13] P. Guo, The emerging field of RNA nanotechnology, Nat. Nanotechnol. 5 (2010) 833–842.
[14] P. Guo, F. Haque, B. Hallahan, R. Reif, H. Li, Uniqueness, advantages, challenges, solutions, and perspectives in therapeutics applying RNA nanotechnology, Nucleic Acid Ther. 22 (2012) 226–245.
[15] D. Jasinski, F. Haque, D.W. Binzel, P. Guo, Advancement of the emerging field of RNA nanotechnology, ACS Nano 11 (2017) 1142–1164.
[16] D. Shu, W.D. Moll, Z. Deng, C. Mao, P. Guo, Bottom-up assembly of RNA arrays and superstructures as potential parts in nanotechnology, Nano Lett. 4 (2004) 1717–1723.
[17] D. Shu, H. Zhang, J. Jin, P. Guo, Counting of six pRNAs of phi29 DNA-packaging motor with customized single-molecule dual-view system, EMBO J. 26 (2007) 527–537.
[18] H. Li, T. Lee, T. Dziubla, F. Pi, S. Guo, J. Xu, C. Li, F. Haque, X.J. Liang, P. Guo, RNA as a stable polymer to build controllable and defined nanostructures for material and biomedical applications, Nano Today 10 (2015) 631–655.
[19] F. Haque, D. Shu, Y. Shu, L.S. Shlyakhtenko, P.G. Rychahou, B.M. Evers, P. Guo, Ultrastable synergistic tetravalent RNA nanoparticles for targeting to cancers, Nano Today 7 (2012) 245–257.
[20] S. Abdelmawla, S. Guo, L. Zhang, S.M. Pulukuri, P. Patankar, P. Conley, J. Trebley, P. Guo, Q.X. Li, Pharmacological characterization of chemically synthesized monomeric phi29 pRNA nanoparticles for systemic delivery, Mol. Ther. 19 (2011) 1312–1322.
[21] J. Liu, S. Guo, M. Cinier, L.S. Shlyakhtenko, Y. Shu, C. Chen, G. Shen, P. Guo, Fabrication of stable and RNase-resistant RNA nanoparticles active in gearing the nanomotors for viral DNA packaging, ACS Nano 5 (2011) 237–246.
[22] D. Shu, Y. Shu, F. Haque, S. Abdelmawla, P. Guo, Thermodynamically stable RNA three-way junction for constructing multifunctional nanoparticles for delivery of therapeutics, Nat. Nanotechnol. 6 (2011) 658–667.
[23] H. Zhang, J.A. Endrizzi, Y. Shu, F. Haque, C. Sauter, L.S. Shlyakhtenko, Y. Lyubchenko, P. Guo, Y. Chi, Crystal structure of 3WJ core revealing divalent ion-promoted thermostability and assembly of the Phi29 hexameric motor pRNA, RNA 19 (2013) 1226–1237.
[24] C. Xu, F. Haque, D.L. Jasinski, D.W. Binzel, D. Shu, P. Guo, Favorable biodistribution, specific targeting and conditional endosomal escape of RNA nanoparticles in cancer therapy, Cancer Lett. 414 (2018) 57–70.
[25] Q. Yu, P. Purwaha, K. Ni, C. Sun, S. Mallik, S.Y. Qian, Characterization of novel radicals from COX-catalyzed arachidonic acid peroxidation, Free Radic. Biol. Med. 47 (2009) 568–576.
[26] Y. Xiao, Y. Gu, P. Purwaha, K. Ni, B. Law, S. Mallik, S.Y. Qian, Characterization of free radicals formed from COX-catalyzed DGLA peroxidation, Free Radic. Biol. Med. 50 (2011) 1163–1170.
[27] Y. Gu, Y. Xu, B. Law, S.Y. Qian, The first characterization of free radicals formed from cellular COX-catalyzed peroxidation, Free Radic. Biol. Med. 57 (2013) 49–60.

[28] Y. Xu, J. Qi, X.Y. Yang, E. Wu, S.Y. Qian, Free radical derivatives formed from COX-catalyzed DGLA peroxidation can attenuate colon cancer cell growth and enhance 5-FU's cytotoxicity, Redox Biol. 2 (2014) 610–618.
[29] Y. Xu, X.Y. Yang, P.J. Zhao, Z.Y. Yang, C.H. Yan, B. Guo, S.Y. Qian, Knockdown of delta-5-desaturase promotes the anti-cancer activity of dihomo-γ-linolenic acid and enhances the efficacy of chemotherapy in colon cancer cells expressing COX-2, Free Radic. Biol. Med. 96 (2016) 67–77.
[30] X. Yang, Y. Xu, A. Brooks, B. Guo, K.W. Miskimins, S.Y. Qian, Knockdown delta-5-desaturase promotes the formation of a novel free radical byproduct from COX-catalyzed ω − 6 peroxidation to induce apoptosis and sensitize pancreatic cancer cells to chemotherapy drugs, Free Radic. Biol. Med. 97 (2016) 342–350.
[31] X. Yang, Y. Xu, T. Wang, D. Shu, P. Guo, K.W. Miskimins, S.Y. Qian, Inhibition of cancer migration and invasion by knocking down delta-5-desaturase in COX-2 overexpressed cancer cells, Redox Biol. 11 (2017) 653–662.
[32] Y. Xu, X. Yang, W. Wang, L. Yang, Y. He, K. Miskimins, S.Y. Qian, Knockdown delta-5-desaturase in breast cancer cells that overexpress COX-2 results in inhibition of growth, migration and invasion via a dihomo-γ-linolenic acid peroxidation dependent mechanism, BMC Cancer 18 (2018) 330.
[33] X. Yang, Y. Xu, D. Gao, L. Yang, S.Y. Qian, Dihomo-γ-linolenic acid inhibits growth of xenograft tumors in mice bearing human pancreatic cancer cells (BxPC-3) transfected with delta-5-desaturase shRNA, Redox Biol. 20 (2019) 236–246.
[34] Y. Xu, X. Yang, D. Gao, L. Yang, K. Miskimins, S.Y. Qian, Dihomo-γ-linolenic acid inhibits xenograft tumor growth in mice bearing shRNA-transfected HCA-7 colony 29 cells targeting delta-5-desaturas, BMC Cancer (2018) (In press).
[35] Y.K. Oh, T.G. Park, siRNA delivery systems for cancer treatment, Adv. Drug Deliv. Rev. 61 (2009) 850–862.
[36] A. Singh, P. Trivedi, N.K. Jain, Advances in siRNA delivery in cancer therapy, Artif. Cells Nanomed. Biotechnol. 46 (2018) 274–283.
[37] W. Guo, W. Chen, W. Yu, W. Huang, W. Deng, Small interfering RNA-based molecular therapy of cancers, Chin. J. Cancer 32 (2013) 488–493.
[38] Y.L. Lyubchenko, L.S. Shlyakhtenko, AFM for analysis of structure and dynamics of DNA and protein-DNA complexes, Methods 47 (2009) 206–213.
[39] O. Quehenberger, A. Armando, D. Dumlao, D.L. Stephens, E.A. Dennis, Lipidomics analysis of essential fatty acids in macrophages, Prostaglandins Leukot. Essent. Fatty Acids 79 (2008) 123–129.
[40] J.A. Abels, F. Moreno-Herrero, T. van der Heijden, C.F. Dekker, N.H. Dekker, Single-molecule measurements of the persistence length of double-stranded RNA, Biophys. J. 88 (2005) 2737–2744.